5M.5

SIERRA ROTORS: A STUDY OF THE IOP 8 ROTOR EVENT

Vanda Grubišić* and Brian J. Billings
Desert Research Institute, Reno, NV

1. INTRODUCTION

Atmospheric rotors, low-level horizontal vortices that form downstream of and parallel to the crest of a mountain range in close association with large-amplitude mountain waves, can pose severe aeronautical hazards and have been cited as contributing to numerous aircraft upsets and accidents involving commercial, military, and civilian aviation (Carney et al. 1988). On the dry lee sides of mountain ranges, rotor circulations can be important for the lofting and transport of aerosols and chemical and biological contaminants (Reid et al. 1993). Despite their considerable impact on human activity, and in contrast to the attendant mountain waves, rotors remain relatively poorly understood atmospheric phenomenon. One reason that so little is known about the dynamics of rotors and their internal structure is that it is very hard to measure the flow within a rotor. Rotors are difficult to sample using in-situ aircraft measurements, and they are intermittent phenomena that are too small in spatial scale to be routinely sampled by conventional observing networks.

A brief historical overview of early studies of rotors is given in Grubišić and Lewis (2004) and Hertenstein and Kuettner (2005). Most of the previous observational evidence and scientific documentation of rotors comes from the Sierra Wave and the Mountain Wave-Jet Stream Projects in the 1950's (Holmboe and Klieforth 1957) as well as the Colorado Lee Wave Program of the late 1960's and early 1970's (Lilly and Toutenhoofd 1969). Recently, rotors have received renewed attention due in part to advances in high-performance computing that have made non-hydrostatic model simulations possible at the resolutions needed to numerically resolve them (Clark et al. 2000, Doyle and Durran 2002, 2004; Chen et al. 2004; Vosper 2004; Grubišić and Billings 2005), and in part to the advances in remote-sensing instrumentation and observational techniques that now allow documentation of rotors, sub-rotor structures and zones of upper-level gravity wave breaking with ground-based and airborne remote sensors (Clark et al. 1994, 2000; Ralph et al. 1997; Cohn et al. 2005).

2. SIERRA ROTORS PROJECT

The Sierra Rotors Project (SRP) is the first, exploratory phase of a coordinated multi-year effort to study mountain waves, rotors, and the attendant phenomena in complex terrain. Part of the SRP goals were to establish quantitative characteristics of the rotor behavior in the lee of the Sierra Nevada including the rotor type, location and the frequency distribution of the related mountain-wave events, as well as to determine the extent to which current operational mesoscale models can reliably forecast the occurrence of rotors, to aid in the preparation for a more extensive T-REX field and research effort (Grubišić and Kuettner 2005).

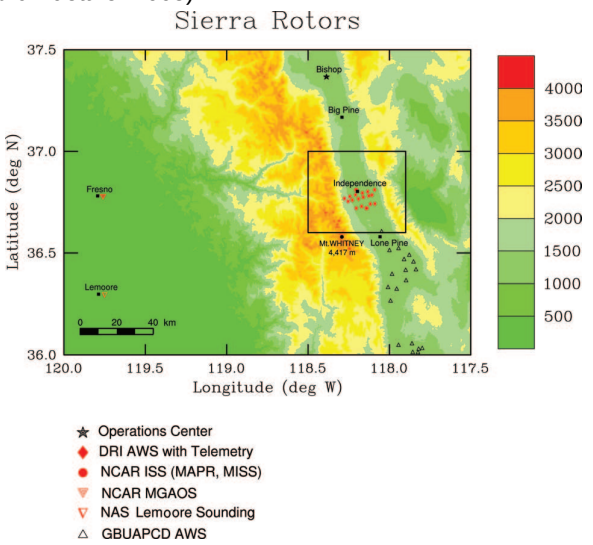

FIG. 1: The Sierra Rotors project field area with deployed SRP ground-based instrumentation marked with red symbols.

The Special Observation Period (SOP) of SRP took place in March and April 2004. The central portion of Owens Valley, near the town of Independence was the site of the SOP activities (Fig. 1). Owens Valley is a narrow U-shaped valley in eastern California, approximately NNW-SSE oriented and bounded by the highest portion of the Sierra Nevada (>4 km) to the west and by the ~ 3-km high White-Inyo range to the east. On the western side of the valley, a gently sloped alluvial fan (~5 km wide) provides a transition from the flat bottom of the valley (at ~1,100 m) to the steep (≈ 30 degrees) eastern slopes of the Sierra Nevada. There is no such transition on the eastern side of the valley where the Inyo range rises steeply from the valley floor.

The core of the instrumentation deployed in SRP in Owens Valley consisted of the long-term DRI surface network of 16 automated weather stations (AWS) with telemetery arranged in three approximately parallel cross-valley transects, and two NCAR/EOL Integrated Sounding Systems (ISS) placed close to the center of the valley, near the northern and southern end of the surface network area (Fig. 2). An ISS consists of a 915

*Corresponding author address: Dr. Vanda Grubišić, Division of Atmospheric Sciences, Desert Research Institute, Reno, NV 89512; e-mail: Vanda.Grubisic@dri.edu

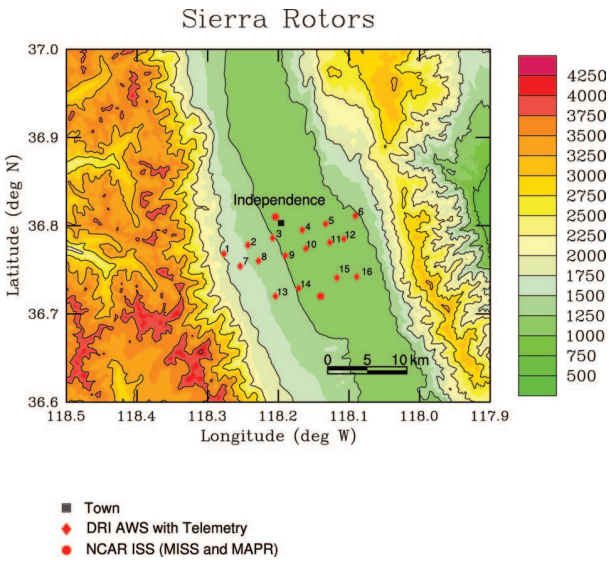

FIG. 2: An enlargement of the central portion of Owens Valley and the southern Sierra Nevada showing the DRI ground AWS network and the location of two NCAR ISS deployed in the Sierra Rotors project. Both ISS were at the marked locations during IOP 8.

MHz boundary-layer radar wind profiler, a Radio Acoustic Sounding System (RASS) for temperature profiling, and surface sensors for wind, temperature, relative humidity, and radiation, and a balloon-borne radiosonde sounding system. In addition to the instruments in Owens Valley, two GPS special sounding sites were located in the Central Valley upwind. The NCAR/EOL mobile GPS atmospheric sounding system (MGAOS) was based in Fresno. The other (fixed) site was at the Naval Air Station Lemoore. The SRP SOP, including all the deployed instrumentation, is described in more detail in Grubišić and Kuettner (2004).

3. IOP 8

Intensive Observation Period (IOP) 8 was organized during a 3-day period of synoptically strongly disturbed weather between 24 and 27 March 2004 that lead to strong mountain wave activity in the lee of the southern Sierra Nevada. This was a well forecast event with a high degree of consistency among forecasts of various models that were followed within the real-time forecasting effort in SRP.

The extended IOP 8 covered the 48-hour period from 18 UTC March 24 to 18 UTC March 26 with a core 24-hour period between 12 UTC March 25 and 12 UTC March 26. During the core IOP, the frequency of radiosonde launches upstream of the Sierra Nevada and within the valley was increased from every 6 hours in the extended IOP to every 3 hours.

3.1 *Synoptic Overview*

The synoptic pattern during IOP 8 was characterized by a strong cross-barrier flow and pre-frontal stability that has previously been identified as conducive to strong mountain-wave generation in the lee of the southern Sierra Nevada (Holmboe and Klieforth 1957). The West Coast upper-air pattern at the start of IOP 8 (18 UTC March 24) was dominated by a closed low off the coast of British Colombia and an associated shortwave trough that extended sufficiently far south to bring SW flow over the southern Sierra Nevada. This disturbed flow steered two different surface cyclones onto the US west coast during the next seventy two hours. The trailing cold front of the first storm dissipated before it reached the west coast of California. The second cyclone and its trailing cold front began to move onshore at 00 UTC March 26. The surface system was followed by the eastward propagation of the upper-level trough, creating strong winds over the southern Sierra Nevada and leading to advection of ample moisture over the area. The peak of this event, with a surface-reaching rotor, was reached several hours before the cold frontal passage at 09 UTC March 26.

4. OBSERVATIONS AND NUMERICAL MODEL SIMULATIONS

In this study we have primarily used the SRP surface network, wind profiler, and radiosonde data, in combination with real-data high-resolution simulations with the Naval Research Laboratory's (NRL) Coupled Ocean-Atmosphere Modeling Prediction System (COAMPS^{TM}; Hodur 1997).

The DRI surface station network provides 30-second data for pressure, temperature, relative humidity and 10-meter winds. The stations' sensors are sampled every 3 seconds, and the data is temporally averaged over 30-second non-overlapping intervals.[1]

The two ISS in SRP SOP were the Multiple Antenna Profiler/ISS (MAPR/ISS or MAPR; Cohn et al. 2001) and the Mobile Integrated Sounding System (MISS; Cohn et al. 2005). MAPR measures the wind vector while pointing continuously in the vertical, providing a horizontal wind vector every few minutes (5-min is typical) and a vertical measurement every dwell (≈30 seconds), whereas MISS has a more traditional boundary-layer wind profiler, providing consensus wind vectors every 30 minutes.[2] More information on wind profiler observations during IOP 8 is given in Cohn et al. (2005).

The real-data high-resolution numerical simulations of the IOP 8 event were performed with the Naval Research Laboratory's (NRL) Coupled Ocean-Atmosphere Modeling Prediction System (COAMPS^{TM}; Hodur 1997). The runs discussed here were carried out on six stationary nested domains with resolutions of 81, 27, 9, 3, 1, and .33 km. Sixty vertical sigma levels were used with finer resolution in the lower levels, the model top at 34.8 km, and a 10.4 km thick absorbing layer at the top. The NRL's Naval Operational Global Atmospheric Prediction

[1] The temporally-averaged data is sent via radio communication to the base station in Independence, and from there, via Internet to the central repository at DRI, where it is displayed in near real-time (http://www.wrcc.dri.edu/trex/)

[2] Quick look plots of SRP data from all NCAR systems in SRP are available at http://www.atd.ucar.edu/rtf/projects/srp2004/.

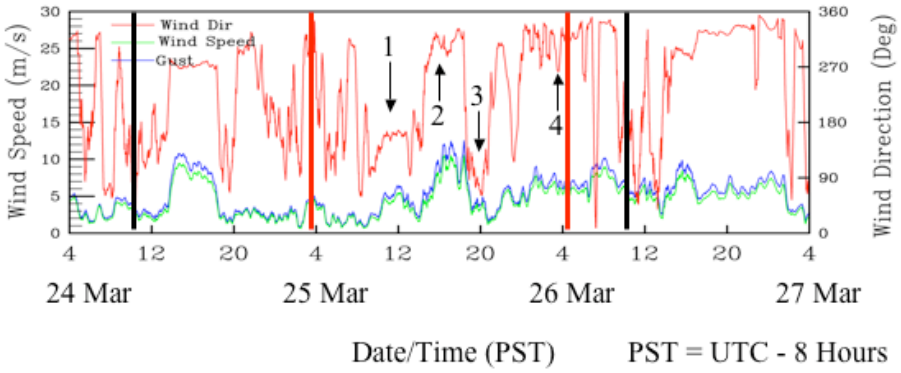

FIG. 3: The time series of wind measurements at station 4 of the DRI network during 24 to 27 March 2004. The thick black and red vertical lines bracket, respectively, the extended and the core IOP 8 period. Time periods labeled 1 to 4 are discussed in more detail in the text.

System (NOGAPS) data was used for initial conditions and 6-hourly boundary updates. The IOP 8 simulation began with a 12 hour "cold" start at 12 UTC March 23 and was followed by three consecutive 24-hour "warm" initializations, the first one of which began at 00 UTC March 24. The choice of the physical parameterizations for these simulations is described in more detail in Grubišić and Billings (2005).

5. RESULTS

5.1 *Temporal Evolution*

Within the 48 hours of the extended IOP, a strong diurnal component of the flow variability was noted in the surface and wind profiler observations, characterized by the presence of thermal circulation patterns in the first part of the day, intensification of the westerly winds in the valley each afternoon, leading to transitions to easterly winds (reversed flow) in the late afternoon at the valley floor. This variability is illustrated in Fig. 3 with the 3-day wind record from station 4. This station lies along the northern line of the DRI surface station network, close to the valley center.

In the following, we examine more closely this diurnal variation of the flow and describe the observed and simulated conditions on the lee side of the Sierra Nevada during four time periods (labeled 1-4 in Fig. 3) within the core IOP.

5.1.1 PERIOD 1: DECOUPLED FLOW

During the late morning and early afternoon hours of the core IOP (14–22 UTC[3] thermally-forced flow patterns were observed within the valley characterized by southeasterly, upslope winds over the alluvial fan, and southerly, up-valley flow along the valley floor (Fig. 4a). The model simulation reproduced these thermally-forced flow patterns, although the timing of transitions from the generally northerly flow of the early morning to the southerly or southeasterly winds of the mid day were more accurately captured along the gentle western slope than in the flat part of the valley.

While winds at the surface were relatively weak and thermally-forced, upper-air soundings during this period showed that winds were quite strong aloft. The wind profilers captured the southerly flow below 2 km AGL, and fairly large alternating positive and negative vertical velocities at 3–4 km AGL (Fig. 5). Broad spectral widths (an indication of strong wind shear and/or turbulence) were observed at those same heights.

After frontal passage, both the wind speed and stability profile became more uniform in the upstream soundings, supporting vertical propagation of wave energy. This change in wave propagation regime was observed by wind profilers in Owens Valley and simulated by COAMPS, as discussed in the previous section on wave breaking aloft. It is important to note that observed and simulated rotors appeared only in the wave trapping periods of the IOP.

The cross-valley vertical sections of the model solution reveal short wavelength trapped lee waves between 3 and 6 km ASL, and a deep layer of much slower decoupled thermally-forced flow within Owens Valley (Fig. 6a).

5.1.2 PERIOD 2: STRONG DOWNSLOPE WINDS

A sharp transition from the thermally-forced flow to strong surface westerlies occurred around 22 UTC, and marked the beginning of a period with strong ($>$10 m s^{-1}) downslope winds in the valley (22–03 UTC), captured by the northern line of the DRI surface network (Fig. 4b), as well as MISS. This transition was particularly sharp along the northernmost line of surface stations. At station 4, the westerly winds at the ground reached their maximum strength at approximately 01 UTC March 26. An extensive wave cloud and föhn gap were visible in the GOES satellite images during this time, and substantial wave clouds and a roll cloud were observed from the valley floor.

During this time, the wind profilers continued to see updrafts and broad spectral widths around 3–4 km AGL, but the same was observed at other altitudes below this

[3]PST=UTC - 8 hours

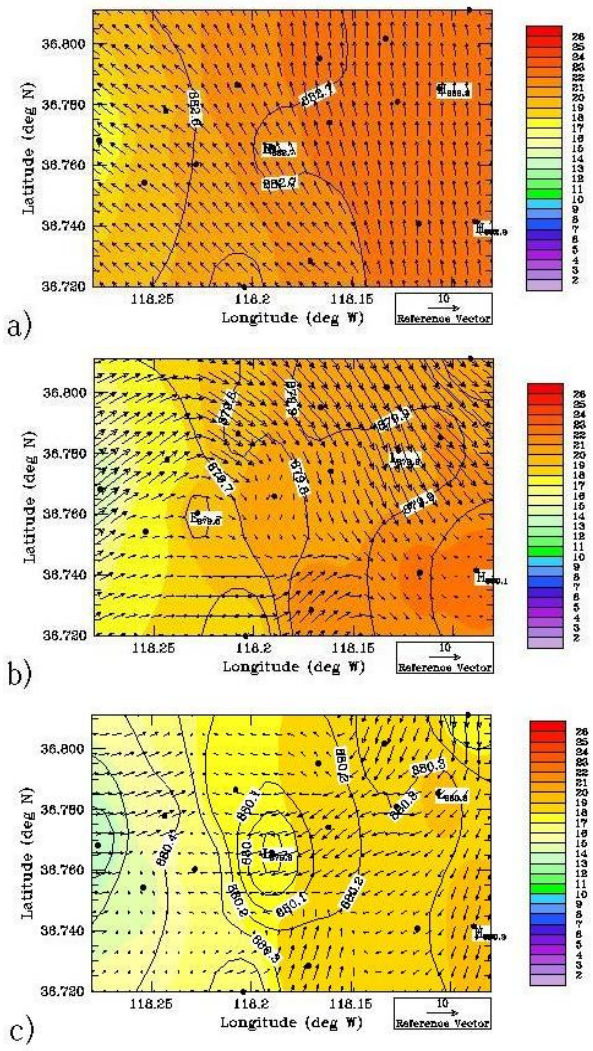

FIG. 4: Surface observations by the DRI mesonetwork (black dots) of temperature (°C in color), wind vectors, and reduced pressure (hPa) at (a) 21 UTC 25 March, (b) 01 UTC 26 March, and (c) 03 UTC 26 March.

level all the way to the ground (Fig. 5). The rawinsonde launched from the valley floor at 00 UTC March 26 was caught in strong wave and rotor updrafts and downdrafts, and descended for a period of time during its flight.

The model vertical cross-sections reveal a longer wavelength trapped lee wave with the lee wave trough and the associated westerly downslope winds penetrating into the valley along the eastern Sierra slope (Fig. 6b).

5.1.3 PERIOD 3: "FOOTPRINT" OF A ROTOR

Two hours later, while winds remained westerly at stations along the western slope, stations in the middle of the valley began to observe an easterly wind. This is strongly suggestive of the horizontal circulation of a rotor reaching the valley floor. A lee-wave induced low-pressure perturbation forcing the reversed, easterly, flow at the ground is evident in the reduced pressure field (Fig. 4c).

The wind profilers continued to observed broad spectral widths extending to the valley floor during this period. This is likely a reflection of the intense turbulence associated with the rotor zone. (The earlier spectral width observations were likely more associated with strong wind shear at the mountain top level.)

A rotor circulation is seen in the model simulation, one hour after it was observed by observations. Underneath the mountain wave crest, the flow has an easterly component and vertical isentropes (Fig. 6c), indicating a horizontal circulation and strong mixing. However, the simulated rotor does not extend to the valley floor, as seen in the observations.

5.1.4 PERIOD 4: WAVE BREAKING ALOFT

The strongest vertical velocities of the extended IOP were observed after frontal passage at 11-12 UTC 26 March. At 2.7 km AGL, MAPR recorded updrafts of 6 m s^{-1}, as well as a downdraft of 5 m s^{-1}, in association with broad spectral widths (Fig. 5). The 12 UTC rawinsonde launch from MAPR also recorded strong negative ascent rates. This strong wave activity was spread over a large vertical distance.

The model cross-sections near this time show a transition from predominant wave trapping to vertically propagating wave energy. At 14 UTC, the mountain wave was located over the Sierra Nevada crest, and vertical isentropes indicate that wave breaking has occurred (see Fig. 5 of Billings and Grubišić 2005; companion paper 5M.6). This corresponds with the strong vertical velocities and broad spectral widths observed by the wind profilers.

After frontal passage, both the wind speed and stability profile became more uniform in the upstream soundings, supporting vertical propagation of wave energy. This change in wave propagation regime was observed by wind profilers in Owens Valley and simulated by COAMPS, as discussed in the previous section on wave breaking aloft. It is important to note that observed and simulated rotors appeared only in the wave trapping periods of the IOP.

After frontal passage, both the wind speed and stability profile became more uniform in the upstream soundings, supporting vertical propagation of wave energy. This change in wave propagation regime was observed by wind profilers in Owens Valley and simulated by COAMPS, as discussed in the previous section on wave breaking aloft. It is important to note that observed and simulated rotors appeared only in the wave trapping periods of the IOP.

5.2 *Upstream Atmospheric Structure*

Upstream soundings taken from MGAUS on the early morning of 25 March show significant wind shear in a layer between the mountain top height and ≈ 500 hPa. Also at 500 hPa, a dry-adiabatic layer served to create a strong decrease in stability. The combination of decreasing stability and increasing wind speed would support the trapping of wave energy in lower levels (Scorer 1949), which is observed in the model cross-sections. In

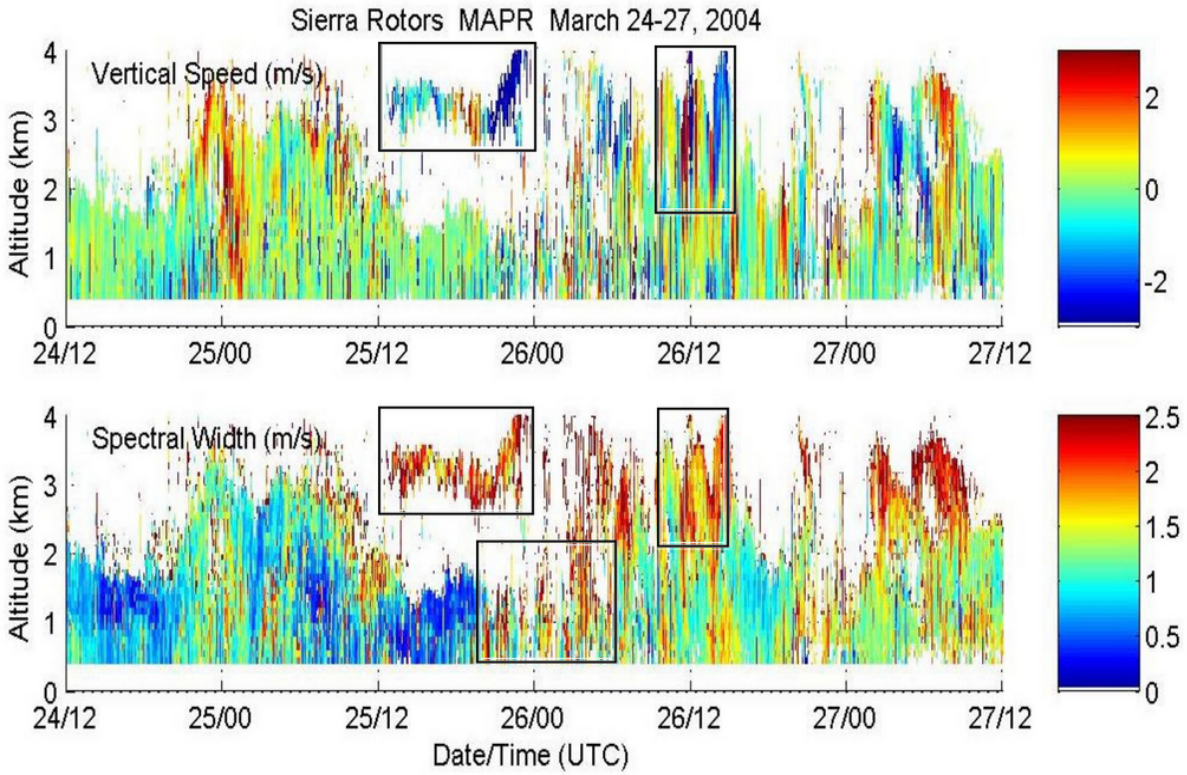

FIG. 5: Time height cross-section of vertical velocity and Doppler spectral width observed with MAPR for 72 hour period encompassing IOP 8 from 12 UTC on March 24 through 12 UTC on March 27. Altitudes are above ground level (AGL). Boxes mark times and features discussed in the text.

addition, a more detailed analysis of the sounding observations shows weak inversions near the mountain crest level at times when strong surface westerlies where occurring in Owens Valley.

After frontal passage, both the wind speed and stability profile became more uniform in the upstream soundings, supporting vertical propagation of wave energy. This change in wave propagation regime was observed by wind profilers in Owens Valley and simulated by COAMPS, as discussed in the previous section on wave breaking aloft. It is important to note that observed and simulated rotors appeared only in the wave trapping periods of the IOP.

6. CONCLUSIONS

An intense mountain wave and rotor event was observed during the Sierra Rotors Project IOP 8 (18 UTC March 24 to 18 UTC March 26). A strong diurnal component of the flow variability was captured by the surface and wind profiler observations during seventy two hours of Sierra perpendicular synoptic flow during which waves were present over Owens Valley. This diurnal cycle was characterized by the presence of thermal circulation patterns in the valley in the first part of the day, decoupled from the trapped lee waves aloft, and the intensification of waves and the penetration of westerly winds into the valley each afternoon, leading to transitions to easterly winds (reversed flow) at the valley floor in the late afternoon and early evening. Based on all the available observations, this surface reversed flow most likely represents a footprint of the rotor.

This three-day long event was simulated with the COAMPS model at a very high horizontal resolution ($\Delta x = 300$ m). The COAMPS simulation reproduced well the timing and spatial structure of many of the observed phenomena, and thus could be used to link measurements obtained by the surface network with the remotely-sensed wind profiler observations. Only elevated rotors were simulated in this case—the observations of the rotor-induced reversed flow at the ground were not reproduced by the model simulation. The model also over predicted the strength of the lee side downslope winds.

Two wave regimes were present during the IOP 8 event. In the pre-frontal environment, wave energy trapping dominated, promoted by the mountain-top inversion and decreasing stability above 500 hPa together with the positive wind shear throughout this layer. The horizontal wavelength of trapped lee waves changed considerably during this event. In the post-frontal environment, characterized by more uniform stability and wind profiles, vertical wave energy propagation was possible and the model solutions produced wave-breaking between 6 and 7 km. In this event, rotors formed in the first wave propagation regime, underneath the first crest of a trapped lee wave, at times when these waves were in resonance

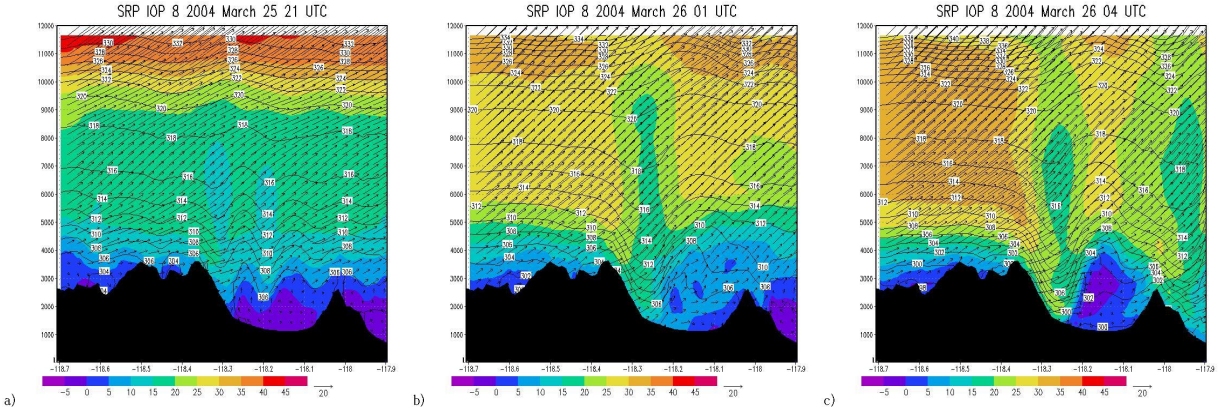

FIG. 6: Vertical cross-sections of horizontal wind vectors (m s^{-1}), isentropes (K), and zonal wind speed (m $^{-1}$ in color) through the northern line of stations at (a) 21 UTC 25 March, (b) 01 UTC 26 March, and (c) 04 UTC 26 March.

with the terrain forcing. At the peak of the event (03–04 UTC March 26), the wavelength of the resonant wave was equal to the valley width at ridge height (30 km), but resonant waves half that wavelength were present also at other times. Rotors occurred only in the late afternoon hours, adding further evidence that diurnal heating is likely important for wave intensification and development of rotors.

ACKNOWLEDGMENTS

The Sierra Rotors Project web page is hosted at DRI by the Mesoscale Dynamics and Modeling Laboratory (MDML) at http://www.mdml.dri.edu. The high-resolution real-data COAMPS runs were carried out on the MDML 68-processor Sierra cluster that was funded by the NSF grant ATM–0116666. The SRP was a joint effort between DRI, NRL, University of Washington, and NCAR, and was funded in part by the NSF grant ATM–0242886 to DRI. We thank all the participants of the Sierra Rotors Project, but especially Dale Durran, Jim Doyle, Qingfang Jiang, Steven Cohn, Bill Brown and Boro Grubišić, for their efforts during the SRP field phase, and Ming Xiao for the analysis and graphical display of the surface data.

REFERENCES

Carney, T. Q., A. J. Bedard, J. M. Brown, J. McGinley, T. Lindholm, M. J. Kraus, 1988: *Hazardous Mountain Winds and Their Visual Indicators.* US Dept of Transportation, FAA, Washington, D. C. Publication AC 00–57.

Chen, Y., F. L. Ludwig, and R. L. Street, 2004: Stably-stratified flows near a notched, transverse ridge across the Salt Lake Valley. *J. Appl. Meteor.*, **43**, 1308–1328.

Clark, T. L., W. D. Hall, and R. M. Banta, 1994: Two- and three-dimensional simulations of the 9 January 1989 windstorm: Comparison with observations. *J. Atmos. Sci.*, **51**, 2317–2343.

——, ——, R. M. Kerr, D. Middleton, L. Radke, F. M. Ralph, P. J. Nieman, and D. Levinson, 2000: Origins of aircraft-damaging clear-air turbulence during the 9 December 1992 Colorado downslope windstorm: Numerical simulations and comparison with observations. *J. Atmos. Sci.*, **57**, 1105–1131.

Cohn, S. A., W. O. J. Brown, C. L. Martin, M. S. Susedik, G. Maclean, and D. B. Parsons, 2001: Clear air boundary layer spaced antenna wind measurements with the Multiple Antenna Profiler (MAPR), *Annales Geophysicae,* **19,** 845–854.

——, ——, and V. Grubišić, 2005: The Mobile Integrated Sounding System (MISS): Description and lessons from the Sierra Rotors Project. *Proceedings. AMS 13th Symposium on Meteorological Observations and Instrumentation.* Savannah, GA, Amer. Meteor. Soc., http://ams.confex.com/ams/pdfpapers/94055.pdf

——, ——, ——, and B. J. Billings, 2005: The signature of waves and rotors in wind profilers: Results of the Sierra Rotors Project. *Proceedings. AMS 32nd Conference on Radar Meteorology.* Amer. Meteor. Soc., Paper **2R.6**.

Doyle, J. D., and D. R. Durran, 2002: The dynamics of mountain-wave induced rotors. *J. Atmos. Sci.*, **59**, 186–201.

——, and ——, 2004: Recent developments in the theory of atmospheric rotors. *Bull. Amer. Meteor. Soc.*, **85**, 337–342.

Grubišić, V., and J. P. Kuettner, 2005: Final plans for the Terrain-induced Rotor Experiment (T-REX). *Proceedings. AMS 11th Conference on Mesoscale Processes.* Albuquerque, NM, Amer. Meteor. Soc., Paper **JP7J.5**.

——, and ——, 2004: Sierra Rotors and the Terrain-induced Rotor Experiment (T-REX). *Proceedings. AMS 11th Conference on Mountain Meteorology*

and the Annual Mesoscale Alpine Programme Meeting. Bartlett, NH, Amer. Meteor. Soc., http://ams.confex.com/ams/pdfpapers/77384.pdf.

——, and J. Lewis, 2004: Sierra Wave Project revisited: 50 years later. *Bull. Amer. Meteor. Soc.*, **85**, 1127–1142.

——, J. D. Doyle, J. P. Kuettner, G. S. Poulos, and C. D. Whiteman, 2004: Terrain-induced Rotor Experiment (T-REX) Overview Document and Experiment Design. 72 pp. Available at http://www.joss.ucar.edu/trex/.

——, and B. J. Billings, 2005: A numerical study of the Sierra Rotors IOP 8 event. In preparation.

Hertenstein, R. F., and J. P. Kuettner, 2005: Rotor types associated with steep lee topography: Influence of the wind profile. *Tellus A,* **57,** 117–135.

Hodur, R. M., 1997: The Naval Research Laboratory's Coupled Ocean/Atmosphere Mesoscale Prediction System (COAMPS). *Mon. Wea. Rev.,* **111,** 1414–1430.

Holmboe, J. R., and H. Klieforth, 1957: *Investigation of mountain lee waves and the airflow over the Sierra Nevada. Final Report.* Department of Meteorology, UCLA, Contract AF 19(604)-728, 283 pp.

Lilly, D. K., and W. Toutenhoofd, 1969: The Colorado Lee Wave program. In *Clear Air Turbulence and Its Detection,* Plenum Press, 232–245.

Reid, J. S., R. G. Flocchini, T. A. Cahill, R. S. Ruth, and D. P. Salgado, 1993: Local meteorological, transport, and source aerosol characteristics of late autumn Owens Lake (dry) dust storms. *Atmos. Environ.,* **28,** 1699–1706.

Scorer, R. S., 1949: Theory of lee waves of mountains. *Q. J. R. Meteorol. Soc.,* **75,** 41–56.

Vosper, S. B., 2004: Inversion effects on mountain lee waves. *Q. J. R. Meteorol. Soc.,* **130,** 1723–1748.